

Facile Synthesis of three-dimensional Carbon Nanocages with Hierarchical Porous Structures as Supercapacitor Electrode Materials

Liang Jiang^{1,*}, Jing Wang^{2,*}, Yujie Li¹, Qianqian Zhai², Xuyan Mao¹, Xiangyu Xu¹, Jie Yang¹, Shifeng Hou¹

¹ Bio-Nano & Medical Engineering Institute, Jining Medical University, 133 Hehua Road, Jining, 272067, China.

² Physics and Information Engineering Department, Jining University, 1 Xingtian Road, Qufu, 273155, China.

*E-mail: jiangliangjnm@126.com (Liang Jiang), wangjingouc@126.com (Jing Wang).

Received: 2 March 2019 / Accepted: 5 May 2019 / Published: 10 June 2019

Hierarchical carbon with a three-dimensional (3D) structure has become a promising electrode material for supercapacitors due to its excellent rate capability. High surface area hierarchical structure carbon nanocages (HHNCs) were prepared using magnesium oxide as a template with in situ chemical activation. These materials feature a 3D network structure interconnected by carbon nanocages, a high specific surface area ($2073 \text{ m}^2 \text{ g}^{-1}$), a high pore volume ($3.17 \text{ cm}^3 \text{ g}^{-1}$) and a multiscale pore size distribution. Because of the synergistic effects of these advantages, as supercapacitor electrode materials, HHNCs show excellent electrochemical performance with a high specific capacitance (276 F g^{-1} at 0.05 A g^{-1}) and an excellent rate capability (205 F g^{-1} at 20 A g^{-1}). This makes HHNCs promising supercapacitor electrode materials with many potential applications.

Keywords: Supercapacitor; Carbon nanocages; Hierarchical structure; Hard template; In situ chemical activation.

1. INTRODUCTION

Since the oil crisis in the 1970s, environmental pollution has become increasingly serious, and energy shortages have become a great challenge for human society. However, solar energy, wind energy and other renewable energies depend on natural conditions. These renewable energies have characteristic nonuniformity and inconsistent timeliness of power output, which leads to instability of power output. Therefore, energy storage devices are needed to make up for the shortcomings of these clean energy

sources, and energy conversion technology has attracted increasing attention. Supercapacitors have many advantages, such as high-power density, long life cycles, fast charging speeds, less pollution, and increased safety and reliability. Supercapacitors have become a new type of energy storage of great interest [1-3]. The key factors affecting the capacitive performance of carbon materials include specific surface area, crystal structure, surface functional groups, porous structure and micromorphology [4-6]. A large number of experiments and theories have proven that hierarchical porous carbon is beneficial for increasing the storage capacity of the charge and decreasing charge transfer resistance. Macroporous structures serve as the "warehouse" of the electrolyte, mesoporous structures serve as ion channels, and microporous structures serve as the units of charge storage. The three porous structures play their respective roles so that hierarchical porous carbon materials can exhibit more excellent capacitive properties [7-9]. The synergy between different porous structures makes hierarchical porous carbons exhibit excellent capacitive performance [5, 10]. Three-dimensional (3D) hierarchical porous carbon not only has the electrolyte ion transport advantages of hierarchical porous carbon but also provides a continuous electron transport pathway in the 3D nanoscale architecture, thus ensuring good electronic conductivity. Carbon nanotubes (CNTs) and graphene are synthesized by self-assembly methods to obtain 3D porous carbon materials that exhibit excellent electrical double layer capacitive properties [11, 12]. However, high cost limits the application prospects of these materials. In addition, carbon nanocages (CNCs) are another kind of carbon material with 3D structure. The hollow cavities of carbon nanocages and the interparticle voids become ion-buffering reservoirs of electrolytes that reduce the charge transfer resistance of electrode materials. The energy density and cycle stability of CNCs are at advanced levels in supercapacitors [13-15]. However, the preparation methods of CNCs are still complicated. High performance carbon nanocage electrode materials are usually prepared by chemical vapor deposition and other complex methods [16]. Therefore, it is urgent to develop simple methods to prepare high-performance 3D carbon nanocage materials.

In this study, high surface area hierarchical structure carbon nanocages (HHNCs) are prepared by in situ chemical activation using a hard template method. Magnesium oxide was used as the template, inexpensive sucrose was used as the carbon source, and less corrosive potassium carbonate was used as the chemical activator to prepare hierarchical carbon nanocages. HHNCs combine the advantages of a 3D architecture, hierarchical porous structure, high specific surface area and high oxygen content. The synergistic effects of these factors make HHNCs exhibit excellent capacitive performance. At a current density of 20 A g^{-1} , the specific capacitance value is as high as 205 F g^{-1} . HHNCs are expected to be potential electrode materials for high-performance supercapacitors.

2. EXPERIMENTAL

In a typical experiment, 2 g sucrose, 0.4 g potassium carbonate and 4 g magnesium oxide were mixed in 12 g water. The mixture was continuously stirred and dried at $80 \text{ }^\circ\text{C}$. The mixture was placed in a tubular furnace. Pyrolysis of the mixture was performed in a N_2 atmosphere at $800 \text{ }^\circ\text{C}$ for 2 h. The sample was leached in a 2 M HCl solution at $80 \text{ }^\circ\text{C}$ for 8 h to remove magnesium oxide and washed thoroughly with deionized water. Finally, the sample was dried at $60 \text{ }^\circ\text{C}$ in an oven and was denoted as

HHNC. For comparison, no potassium carbonate was added during the above preparation, and the sample was denoted as HNC.

The morphology and microstructure of the samples were observed via a Zeiss ultra plus scanning electron microscope and an FEI tecnai G2 transmission electron microscope. X-ray photoelectron spectra (XPS) were measured on a Thermo Escalab 250Xi photoelectron spectrometer. Specific surface area and porous texture of the carbons were determined by nitrogen adsorption-desorption measurements at 77 K with a Quantachrome AutoSorb iQ2 system. The specific surface area was obtained by the BET (Brunauer–Emmet–Teller) method, and the pore size distribution of the carbon was calculated using Quenched Solid Density Functional Theory (QSDFT) model.

Carbon, acetylene black and polytetrafluoroethylene (PTFE) were mixed and ground at the weight ratio of 85:10:5. The mixture was sandwiched between two nickel foam current collectors with diameters of 9 mm to fabricate the working electrode. Cyclic voltammetry (CV) and electrochemical impedance spectroscopy (EIS) tests were measured on an electrochemical workstation (Shanghai CH Instruments, CHI760E) in a three electrode cell in 6 M KOH with a Pt plate and with an Ag/AgCl electrode as the counter electrode and reference electrode, respectively. Galvanostatic charge-discharge (GC) tests were carried out on a battery test station (Neware) in a two-electrode system, and two working electrodes were placed on both sides of the polypropylene with polypropylene as the separator; then, the electrodes were sealed with 2032 battery after adding a steel sheet.

The equation $C = \frac{\int I dV}{2Uvm}$ was used to calculate the specific capacitance of the electrode from CV data, where $\int IdV$, U , v and m represent the charge integrated from potential window, the voltage difference, the potential scan rate and the mass of electroactive materials in the electrodes, respectively [17].

The formula $C = \frac{4It}{\Delta Vm}$ was also used to calculate the specific capacitance of the electrode according to charge-discharge curves where m , ΔV , I and t represent the mass of electroactive materials on a two-electrode configuration, voltage drop, discharging current and discharging time, respectively [18].

The formula $C'' = \frac{Z'}{2\pi f m (|Z'|^2 + |Z''|^2)}$ was used to calculate the imaginary capacitance from impedance spectroscopy data, where Z' , Z'' , f and m represent the real component of the electrode resistance, the imaginary component of the electrode resistance, the operating frequency and the mass of the electroactive materials, respectively [19].

3. RESULTS AND DISCUSSION

The SEM micrographs of the magnesium oxide template are shown in Fig. 1. The size of cubic magnesium oxide was ca. 100 nm as shown in Fig. 1a. The magnesium oxide particles were stacked together to form voids. SEM and TEM images of HHNCs are depicted in Fig. 1b and Fig. 1c. The 3D porous carbon was obtained by the reverse replication of the magnesium oxide particles. The hollow cage-like structure with an average diameter of ca. 100 nm was found from TEM, which is due to the removal of magnesium oxide particles. In addition, Fig. 1d shows that the shell thickness of HHNCs was

approximately 5 nm. The thin layer structure of the carbon nanocages resulted in the micropores and mesopores on the pore having a small aspect ratio.

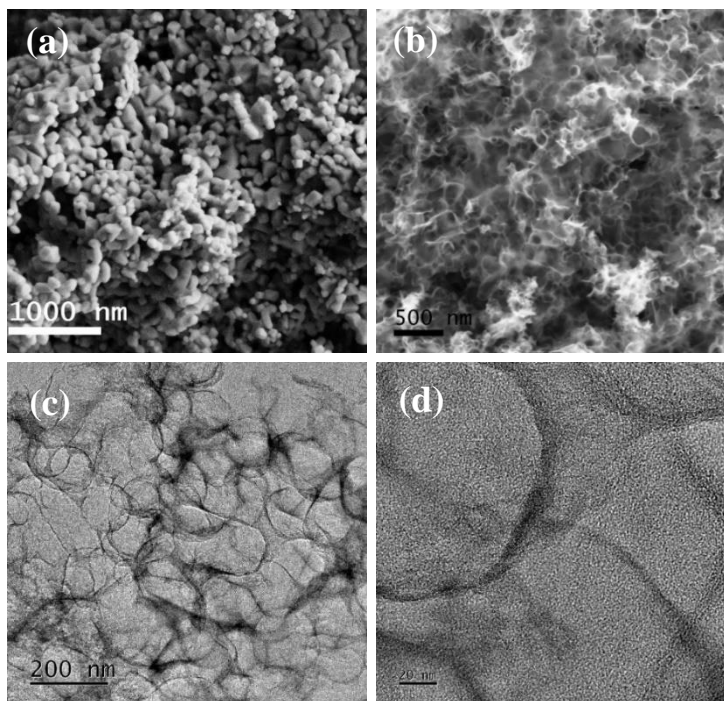


Figure 1. SEM images of magnesium oxide (a) and HHNCs (b), TEM images of HHNCs (c,d).

A porous structure with a small aspect ratio is beneficial to the transport of electrolyte ions [20]. In addition, nanocages are stacked to form 3D micron-sized sponge-like particles, creating interparticle voids with pore sizes over tens of nanometers. Therefore, the macropores of HHNCs contribute to the cavities inside cages and interparticle voids.

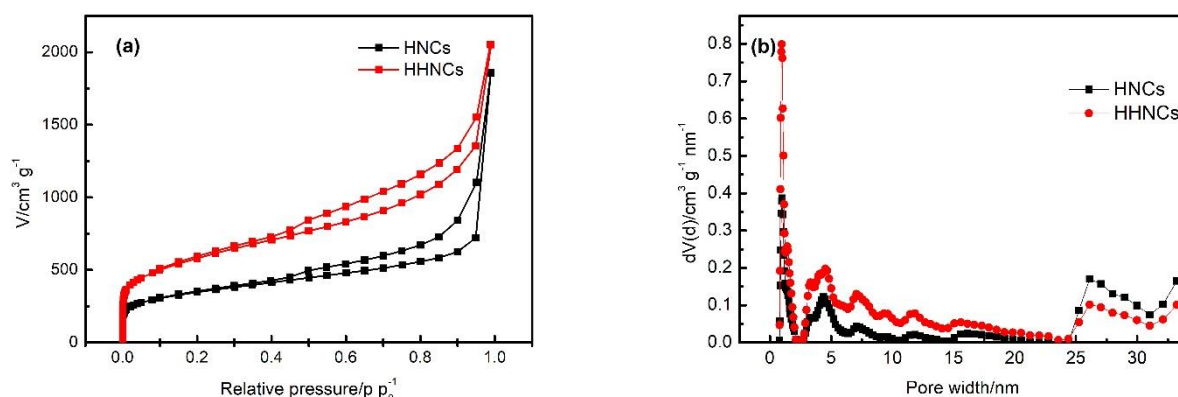


Figure 2. Nitrogen adsorption and desorption isotherms (a) and corresponding pore size distribution curves (b) of HNCs and HHNCs.

Nitrogen adsorption and desorption isotherms were used to study the porous structure of carbon materials (Fig. 2a). Obviously, the HNC and HHNC samples exhibited a type IV adsorption isotherm. Due to the appearance of a hysteresis loop, the existence of mesopores is suggested. In addition, there

was a significant increase in the adsorption capacity at a relative pressure of 0.9-1.0, which is usually associated with macropores in the carbon nanocages [14]. The pore size distribution curves of different samples are shown in Fig. 2b. It can be found that the HNC and HHNC samples show characteristics of microporous and mesoporous hierarchical distribution.

Table 1. Textural properties of HNCs and HHNCs. S_{mic} and S_{ext} are micropore and external surface area, respectively.

Sample	$S_{\text{BET}}(\text{m}^2 \text{g}^{-1})$	$S_{\text{mic}}(\text{m}^2 \text{g}^{-1})$	$S_{\text{ext}}(\text{m}^2 \text{g}^{-1})$	$V_{\text{p}}(\text{cm}^3 \text{g}^{-1})$
HNCs	1237	516	721	2.87
HHNCs	2073	727	1346	3.17

The textural properties of the samples are summarized in Tab. 1. The HHNCs had a specific surface area of $2073 \text{ m}^2 \text{g}^{-1}$ and pore volume of $3.17 \text{ cm}^3 \text{g}^{-1}$. The specific surface area of the HHNC material was 68% higher than that of the HNC material, which is because the activation of potassium carbonate significantly increases the specific surface area, especially the mesoporous and macroporous surface area of carbon nanocages [21]. Potassium carbonate reacted with carbon at high temperatures. During the process, potassium carbonate increased the specific surface area and pore volume by reacting with carbon. The CO and CO₂ produced during the activation process played a role in pore enlargement and significantly increased the mesoporous specific surface area of carbon materials. Additionally, the external area to total surface area ratio of HHNCs reached 64.9%, revealing that HHNCs are mainly mesoporous and macroporous. A large amount of mesoporous structure is conducive to the transport of electrolyte ions [22].

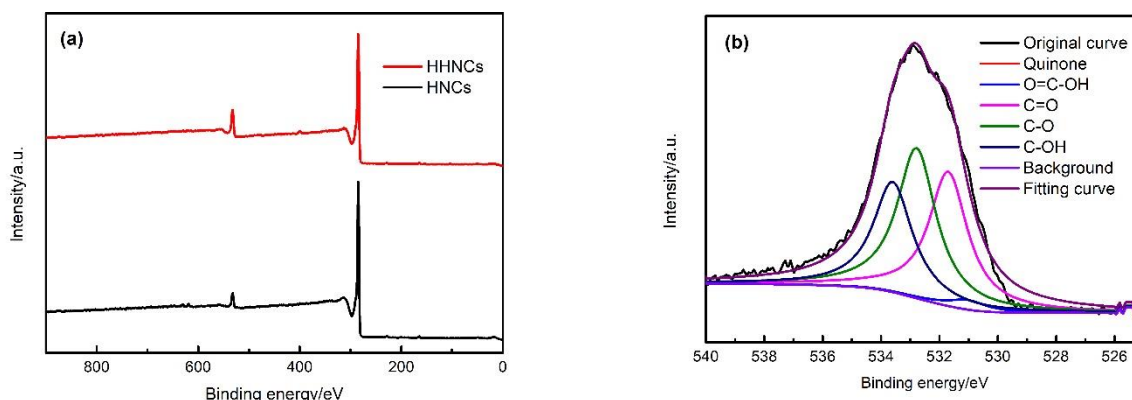


Figure 3. XPS full survey spectra of the carbon (a), High-resolution spectra for O1s of HHNCs (b).

The chemical state of the surface of the carbon material was investigated by XPS. As shown in Fig. 3a, the oxygen content of HHNCs was 9.2 at. %, which is significantly higher than that of HNCs at 5.5 at. %. The oxygen-containing functional group on the surface of the carbon material improved the wettability of the carbon material surface and increased the accessible surface area between the

electrolyte ion and the carbon material surface, thereby further improving the electric double layer performance. In addition, it was also found that in an alkaline electrolyte solution, some oxygen-containing functional groups produced pseudocapacitance via an oxidation-reduction reaction. The high-resolution XPS spectrum of HHNCs is shown in the Fig. 3b. According to the fitting result, the carbon material contained 29.7% hydroxyl and carboxyl functional groups. The hydroxyl and carboxyl functional groups on the surface of the carbon material can react as follows to produce pseudocapacitance, which further improves the capacitive performance of carbon materials [23, 24].

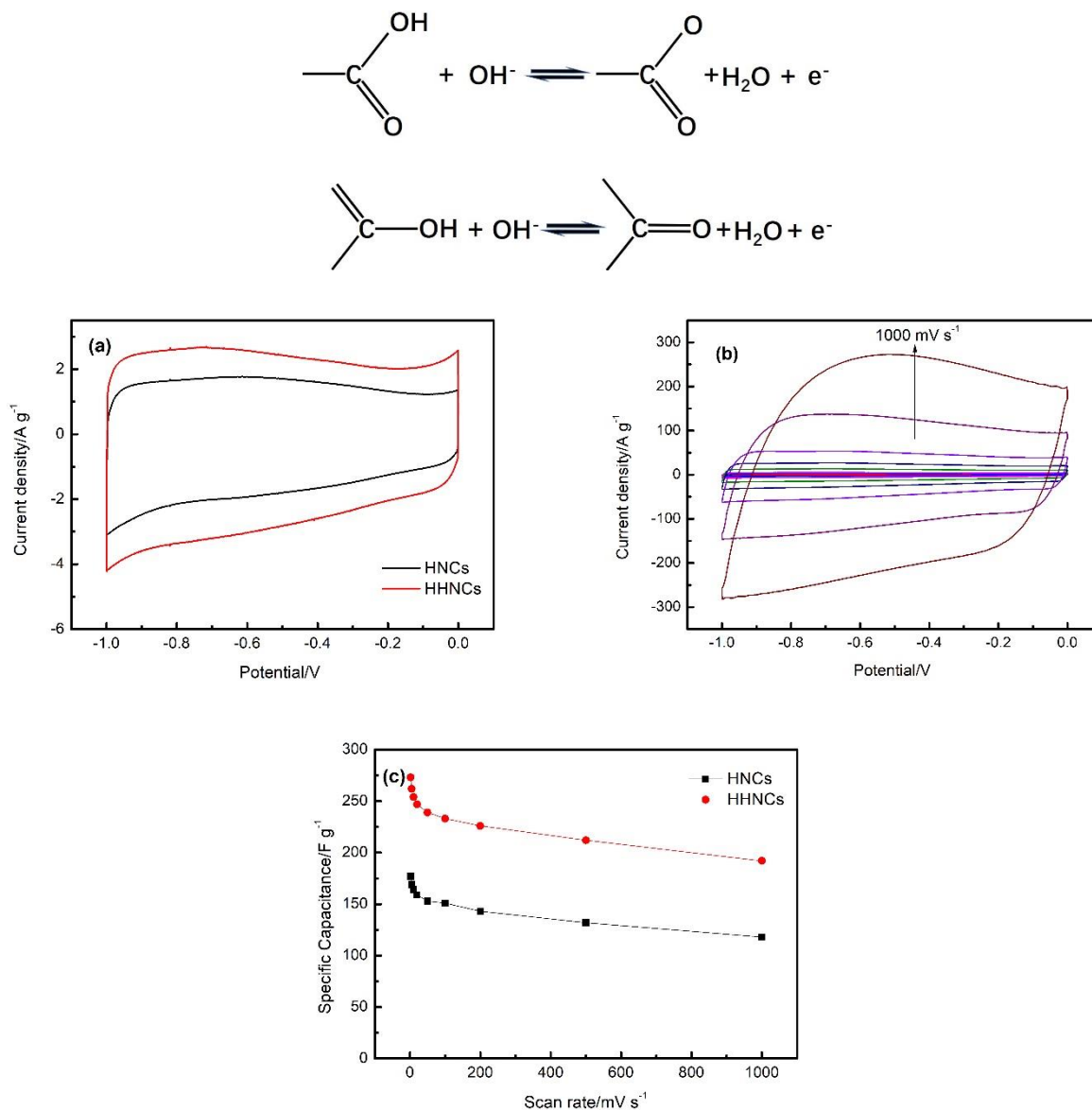


Figure 4. CV curves for HNCs and HHNCs at a scan rate of 10 mV s⁻¹ (a), CV curves of HHNC electrodes at scan rates of 2~1000 mV s⁻¹ (b), Specific capacitance of carbon at different scan rates (c).

The CV curves of HHNCs and HNCs at a scan rate of 10 mV s⁻¹ are shown in Fig. 4a. The rectangular shape of the samples indicates that the carbon nanocage electrode materials have ideal electric double layer capacitive characteristics. The response current of HHNCs was significantly higher

than that of HNCs, indicating that HHNCs have higher capacitance. CV curves of HHNCs at different scan rates are shown in Fig. 4b; the CV curves at a low scan rate exhibited symmetrical rectangular shapes with small humps, revealing that HHNCs demonstrate electric double layer and pseudocapacitive behaviors [25]. Increasing the scan rate to 500 mV s^{-1} and 1000 mV s^{-1} , HHNCs still demonstrated approximately rectangular-like shapes without oblique angles, indicating that ion diffusion in the 3D porous carbons was extremely fast. The specific capacitance of the samples at different scan rates is shown in Fig. 4c. The specific capacitance was 273 F g^{-1} and 177 F g^{-1} for HHNCs and HNCs, respectively, at a scan rate of 2 mV s^{-1} . The high capacitance for HHNCs is mainly due to the high surface area caused by chemical activation. The capacitance per surface area at 2 mV s^{-1} was $14.3 \mu\text{F cm}^{-2}$ for HNCs, which is slightly higher than $13.2 \mu\text{F cm}^{-2}$ for HHNCs. The main reason for the difference is that the two carbons have different porous structures. The micropores are favored for charge accumulation and thereby improve the electrical double layer [26]. The micropore ratio of HNCs was 41.7%, which was higher than 35.1% for HHNCs. More micropores increase the area normalized capacitance of HNCs. Although HHNCs contain more oxygen-containing functional groups, the pseudocapacitance still cannot compensate for the reduction of area normalized capacitance caused by the decrease in microporosity. Thus, the area normalized capacitance is still lower than that of HNCs.

In addition, the diffusion limitation of electrolyte ions in the micropores will reduce the capacitance at high currents [27]. When the scan rate increased to 1000 mV s^{-1} , the specific capacitances of HNCs and HHNCs were 118 F g^{-1} and 192 F g^{-1} , respectively, and the normalized capacitance was $9.5 \mu\text{F cm}^{-2}$ and $9.3 \mu\text{F cm}^{-2}$, respectively. At high currents, it is difficult for electrolyte ions to enter the micropores to form electric double layers due to high transmission resistance, resulting in a decrease in area normalized capacitance. Mesopores and macropores promote ion transport by providing ion transport channels and shortening the diffusion pathway of ions, increasing the area normalized capacitance at high currents. As a result, the gap between the two was significantly reduced at high currents.

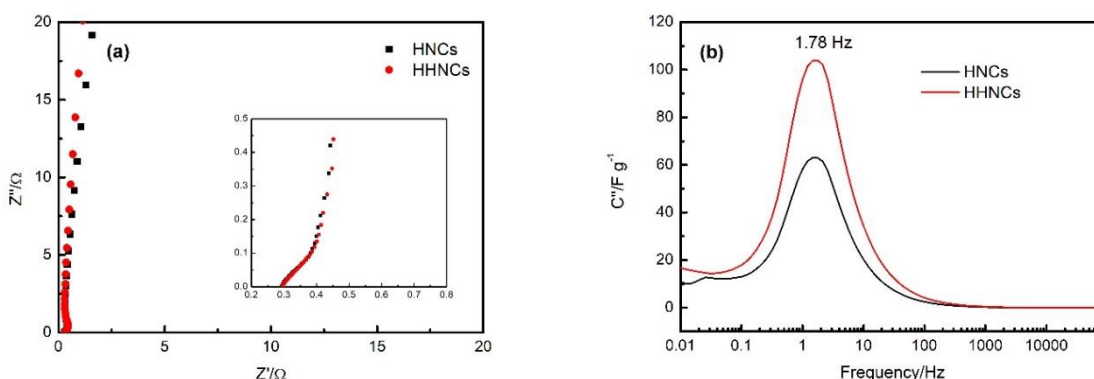


Figure 5. Nyquist plots of HHNCs and HNCs (a), Imaginary part of the capacitance versus the frequency curves of the samples (b).

Fig. 5a shows Nyquist plots of HHNCs and HNCs, which are both perpendicular to the real axis at low frequency regions with the ideal capacitive behaviors. The intercept of the high-

frequency region represents the resistance including contact resistance, electrolyte resistance and the intrinsic resistance of the electrode [28]. The plot shows that the electrode has a low resistance value of 0.29Ω . There were no obvious semicircles at higher frequency regions for HHNCs and HNCs, indicating that fast ion diffusion occurs in the porous electrode material due to the synergistic effect of mesopores and macropores [15]. The data of EIS were further processed based on the modeling of the capacitance in imaginary part (C'') [19]. Fig. 5b shows the curve of the imaginary part of the capacitance with frequency. A maximum value of the imaginary part of the capacitance appeared with the change in frequency. This extreme value was considered as the demarcation point of the electrode's resistive behavior and capacitive behavior. The time constant t_0 is described as the characteristic relaxation time of the entire system, which is equal to $1/f_0$. t_0 is the minimum time to release the energy with an efficiency exceeding 50%. The HHNC electrode exhibited a fast frequency response with a t_0 of 0.56 s. Notably, the value was relatively low compared with the values of the previously reported carbon materials in aqueous electrolytes, such as carbon nanosheets (0.7-1.6 s) [29], 3D hierarchical porous carbon (6.7 s) [30], and extraordinary porous few-layer carbon (4.16 s) [31], signifying smooth mass transfer due to the interconnected hierarchical porous structure of HHNCs.

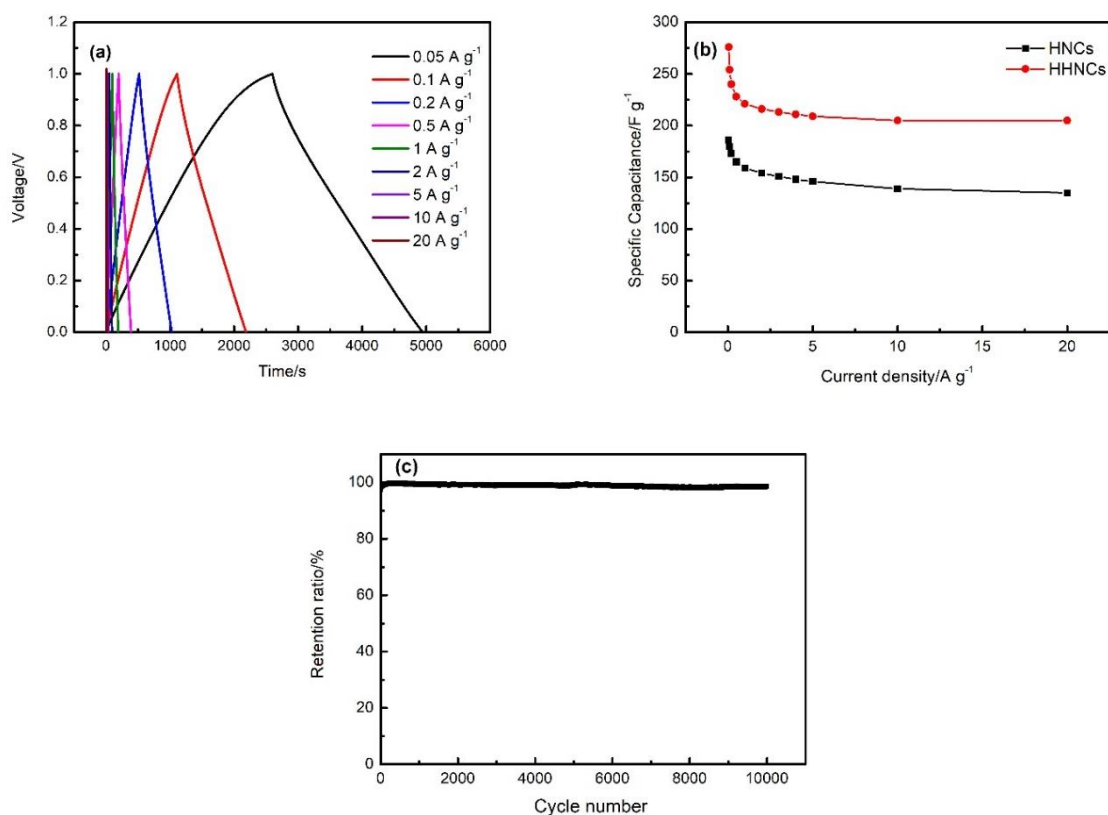


Figure 6. Galvanostatic charge-discharge profiles of HHNCs at different current densities (a), Specific capacitance of carbons at different current densities (b), The cycling stability of HHNCs at a current density of 10 A g^{-1} (c).

Fig. 6a shows galvanostatic charge-discharge curves of HHNCs at different current densities. The slightly deviated isosceles symmetrical triangle confirmed that HHNCs have electric double layers and pseudocapacitive behaviors, which is consistent with the results of CV curves. At the current density of 10 A g^{-1} , no obvious voltage (IR) decrease was observed, indicating low equivalent series resistance. The specific capacitances of the samples at different current densities are shown in Fig. 6b. The specific capacitance of HHNCs was 276 F g^{-1} at a current density of 0.05 A g^{-1} , which is higher than 186 F g^{-1} for HNCs. The specific capacitance of HHNCs achieved values of 254, 221, 207 and 205 F g^{-1} at 0.1, 1, 10 and 20 A g^{-1} , respectively. As shown in Tab. 2, the results were compared with those reported in the literature. HHNCs exhibited better capacitive performance than other hierarchical porous carbons. The excellent capacitive performance of HHNCs can be attributed to their unique structure. The chemical activation of potassium carbonate greatly increases the specific surface area of carbon materials, thereby enhancing the ability of carbon nanocages to store more charge. The 3D nanoscale structure of the interconnected nanocages provides a continuous electron pathway to ensure good electrical conductivity. The mesoporous structure supplies fast ion transport channels, and macroporous frameworks act as ion-buffering reservoirs, thus shortening the ion diffusion pathway. Synergistic effects of the hierarchical porous structure of 3D carbon include high specific capacitance and excellent rate performance.

Table 2. The comparison of capacitive performance of various electrode materials

Sample	Capacitance (F g^{-1})	Current density (A g^{-1})	Electrolyte	Ref
HHNCs	254	0.1	6 M KOH	This work
G/SWCNHs	217	1	1 M KOH	[32]
HPCFs	206	1	6 M KOH	[33]
3D SMG	200	0.5	2 M KOH	[34]
ESCT	229	0.1	6 M KOH	[35]
HPC	181	0.2	6 M KOH	[36]
HPC-2	245	0.1	6 M KOH	[37]

The cyclic stability of the HHNC button cell was measured at a current density of 10 A g^{-1} (Fig. 6c). Clearly, the discharge capacity remained stable, and the capacitance had no obvious reduction. The capacitance retention rate reached up to 98.6% after 10,000 cycles. HHNCs had good cycling stability.

4. CONCLUSIONS

In summary, the HHNC carbon nanocage materials with high specific surface area and hierarchical porous structure were prepared by using sucrose as a carbon precursor with magnesium oxide as a hard template using in situ K_2CO_3 chemical activation. HHNCs have high specific surface area and a 3D hierarchical structure. The interconnected 3D structure improved the overall conductivity of the carbon materials. The synergistic effects of the macropores and mesopores effectively reduced the resistance of electrolyte ion transport. The HHNC electrode for a supercapacitor exhibited a high specific

capacitance of 276 F g⁻¹ at 0.05 A g⁻¹ and an excellent rate capability of 205 F g⁻¹ at 20 A g⁻¹. In addition, the capacitance retention ratio after 10000 cycles reached 98.6%, demonstrating excellent cycling stability. This work provides a simple method to prepare porous carbons with a 3D hierarchical structure for high-performance supercapacitors.

ACKNOWLEDGEMENTS

We gratefully acknowledge the financial support from the National Natural Science Foundation of China (21603084), Natural Science Foundation of Shandong Province (ZR2016BB21, ZR2016BB39, ZR2017BB051, ZR2018PB011) and Projects of medical and health technology development program in Shandong province (2016WS0164), Teachers' research of Jining Medical University (JY2017KJ043, JY2016KJ035Y), A Project of Shandong Province Higher Educational Science and Technology Program (J17KA096, J17KB065, J18KA076) and Talent Team Culturing Plan for Leading Disciplines of University in Shandong Province.

References

1. M. Inagaki, H. Konno and O. Tanaike, *J. Power Sources*, 195 (2010) 7880.
2. Y.G. Wang, Y.F. Song and Y.Y. Xia, *Chem. Soc. Rev.*, 45 (2016) 5925.
3. X.L. Chen, R. Paul and L.M. Dai, *Natl. Sci. Rev.*, 4 (2017) 453.
4. X. Li and B.Q. Wei, *Nano Energy*, 2 (2013) 159.
5. S. Dutta, A. Bhaumik and K.C.W. Wu, *Energ. Environ. Sci.*, 7 (2014) 3574.
6. C.W. Lee, S.B. Yoon, H.K. Kim, H.C. Youn, J. Han, K.C. Roh and K.B. Kim, *J. Mater. Chem. A*, 3 (2015) 2314.
7. D.W. Wang, F. Li, M. Liu, G.Q. Lu and H.M. Cheng, *Angew. Chem. Int. Edit.*, 47 (2008) 373.
8. L. Dong, Z.X. Chen, D. Yang and H.B. Lu, *Rsc Adv.*, 3 (2013) 21183.
9. T.Y. Liu, F. Zhang, Y. Song and Y. Li, *J. Mater. Chem. A*, 5 (2017) 17705.
10. Y. Zhang, T.T. Qu, K. Xiang, Y. Shen, S.Y. Chen, M.J. Xie and X.F. Guo, *J. Mater. Chem. A*, 6 (2018) 2353.
11. Y.Y. Li, Z.S. Li and P.K. Shen, *Adv. Mater.*, 25 (2013) 2474.
12. C. Zhu, T.Y. Liu, F. Qian, T.Y. Han, D.E. B., J.D. Kunzt, C.M. Spadaccini, M.A. Worsley and Y. Li, *Nano Letters*, 16 (2016) 3448.
13. K. Xie, X.T. Qin, X.Z. Wang, Y.N. Wang, H.S. Tao, Q. Wu, L.J. Yang and Z. Hu, *Adv. Mater.*, 24 (2012) 347.
14. J. Zhao, H.W. Lai, Z.Y. Lyu, Y.F. Jiang, K. Xie, X.Z. Wang, Q. Wu, L.J. Yang, Z. Jin, Y.W. Ma, J. Liu and Z. Hu, *Adv. Mater.*, 27 (2015) 3541.
15. L. Jiang, J. Wang, X.Y. Mao, X.Y. Xu, B. Zhang, J. Yang, Y.F. Wang, J. Zhu and S.F. Hou, *Carbon*, 111 (2017) 207.
16. Q. Wu, L.J. Yang, X.Z. Wang and Z. Hu, *Accounts Chem. Res.*, 50 (2017) 435.
17. M. Sevilla and A.B. Fuertes, *Acs Nano*, 8 (2014) 5069.
18. M.D. Stoller and R.S. Ruoff, *Energ. Environ. Sci.*, 3 (2010) 1294.
19. P.L. Taberna, P. Simon and J.F. Fauvarque, *J. Electrochem. Soc.*, 150 (2003) A292.
20. D.W. Wang, F. Li, M. Liu, G.Q. Lu and H.M. Cheng, *J. Phys. Chem.*, 112 (2008) 9950.
21. Y.T. Li, Y.T. Pi, L.M. Lu, S.H. Xu and T.Z. Ren, *J. Power Sources*, 299 (2015) 519.
22. J.S. Lee, S.I. Kim, J.C. Yoon and J.H. Jang, *Acs Nano*, 7 (2013) 6047.
23. Y.J. Oh, J.J. Yoo, Y.I. Kim, J.K. Yoon, H.N. Yoon, J.H. Kim and S.B. Park, *Electrochimica Acta*, 116 (2014) 118.
24. C.M. Chen, Q. Zhang, X.C. Zhao, B.S. Zhang, Q.Q. Kong, M.G. Yang, Q.H. Yang, M.Z. Wang, Y.G. Yang, R. Schöglb and D.S. Su, *J. Mater. Chem.*, 22 (2012) 14076.

25. J.Y. Liang, T.T. Qu, X. Kun, Y. Zhang, S.Y. Chen, Y.C. Cao, M.J. Xie and X.F. Guo, *Appl. Surf. Sci.*, 436 (2018) 934.
26. J. Chmiola, G. Yushin, R. Dash and Y. Gogotsi, *J. Power Sources*, 158 (2006) 765.
27. H. Lu, K.S. Kim, Y.H. Kwon, X.M. Sun, R. Ryoo and X.S. Zhao, *J. Mater. Chem. A*, 6 (2018) 10388.
28. Y.Q. Zhao, M. Liu, P.Y. Tao, Y.J. Zhang, X.T. Gong, Z. Yang, G.Q. Zhang and H.L. Li, *J. Power Sources*, 307 (2016) 391.
29. A.B. Fuertes and M. Sevilla, *Acs Appl. Mater. Inter.*, 7 (2015) 4344.
30. Y. Han, S.X. Liu, D.J. Li and X.F. LI, *Electrochimica Acta*, 138 (2014) 193.
31. M. Qian, Y. Wang, F. Xu, W. Zhao, T.Q. Lin and F.Q. Huang, *Acs Appl. Mater. Inter.*, 10 (2018) 381.
32. K.P. Annamalai, J.P. Gao, L.L. Liu, J. Mei, W.M. Lau and Y.S. Tao, *J. Mater. Chem. A*, 3 (2015) 11740.
33. Y.K. Lv, L.H. Gan, M.X. Liu, W. Xiong, Z.J. Xu, D.Z. Zhu and D.S. Wright, *J. Power Sources*, 209 (2012) 152.
34. L. Chang, D.J. Stacchiola and Y.H. Hu, *Acs Appl. Mater. Inter.*, 9 (2017) 24655.
35. L. Wang, Q.Z. Zhu, J.S. Zhao, Y.B. Guan, J.J. Liu, Z.X. An and B. Xu, *Microporous Mesoporous Mater.*, 279 (2019) 439.
36. H.D. Jiang, X.K. Ye, Y.C. Zhu, L.L. Wang, P. Zhao, Z.Y. Yue, J.L. Xie, Z.Q. Wan and C.Y. Jia, *Appl. Surf. Sci.*, 470 (2019) 573.
37. Q. Li, J.H. Mu, J. Zhou, Y. Zhao and S.P. Zhuo, *J. Electroanal. Chem.*, 832 (2019) 284.

© 2019 The Authors. Published by ESG (www.electrochemsci.org). This article is an open access article distributed under the terms and conditions of the Creative Commons Attribution license (<http://creativecommons.org/licenses/by/4.0/>).